Assessing Small-Signal Grid Strength of 100% Inverter-Based Power Systems

Fuyilong Ma, Huanhai Xin, Senior Member, IEEE, Di Wu, Member, IEEE, Yun Liu, Senior Member, IEEE, and Xia Chen

Abstract—The increasing integration of renewable resources via power electronic inverters is shifting a modern power system toward a 100% inverter-based power system (IBPS). To maintain the stable operation of a 100% IBPS, it is important to identify the small-signal stability issues resulting from the interaction between the power network and inverter-based apparatuses. While grid strength assessment is a useful tool for quickly identifying the small-signal stability issues, the existing methods are not applicable to the 100% IBPS dominated by grid-following (GFL) and grid-forming (GFM) inverters. To fill this gap, the paper proposes a method for assessing small-signal grid strength of the 100% IBPS in order to quickly identify the small-signal stability issues from the perspective of grid strength. First, we formulate a multi-inverter system modeling for the small-signal stability analysis of the 100% IBPS. Then, based on the analysis results, an index is proposed for quantifying grid strength, and its threshold is also analytically defined to characterize the system stability boundary. Also, an analytical expression is derived to determine the threshold and analyze the impacts of GFL and GFM inverters on the stability boundary. With the defined index and its threshold, our method is proposed and then validated on a modified IEEE 39-bus system.

Index Terms—Grid-forming (GFM) inverter, grid strength, generalized short-circuit ratio, grid-following (GFL) inverters, small-signal stability.

I. INTRODUCTION

N THE past decades, power electronics inverters enable a number of various apparatuses, such as rooftop photo-voltaic units, inverter-based resources (IBRs) [1], [2], and voltage source converter-based high voltage direct current

Manuscript received 1 October 2023; revised 18 May 2024 and 7 July 2024; accepted 18 July 2024. Date of publication 23 July 2024; date of current version 25 September 2024. This work was supported in part by the National Key Research and Development Program under Grant 2023YFB2405900, in part by the National Natural Science Foundation of China under Grant U22B6008 and Grant U2166204, and in part by the U.S. National Science Foundation Award under Grant 2333563. Paper no. TPWRD-01377-2023. (Corresponding author: Huanhai Xin.)

Fuyilong Ma and Huanhai Xin are with the College of Electrical Engineering, Zhejiang University, Hangzhou 310027, China (e-mail: 12210001@zju.edu.cn; xinhh@zju.edu.cn).

Di Wu is with the Department of Electrical and Computer Engineering, North Dakota State University, Fargo ND 58102 USA (e-mail: di.wu.3@ndsu.edu).

Yun Liu is with the School of Electric Power Engineering, South China University of Technology, Guangzhou 510641, China (e-mail: liuyun19881026@gmail.com).

Xia Chen is with the School of Electrical and Electronic Engineering, Huazhong University of Science and Technology, Wuhan 430074, China (e-mail: cxhust@hust.edu.cn).

Color versions of one or more figures in this article are available at https://doi.org/10.1109/TPWRD.2024.3432582.

Digital Object Identifier 10.1109/TPWRD.2024.3432582

(VSC-HVDC), to be integrated into the electric power grid [3], [4]. Currently, most inverters are synchronized with the grid via phase locked loop (PLL) modules (hereafter, the PLL-based inverters are referred to as grid-following (GFL) inverters). The synchronizing mechanism of GFL inverters is sensitive to the terminal voltage in a weak AC grid [5], [6], [7], [8], [9]. Alternatively, grid-forming (GFM) inverters are proposed since they can increase the voltage support capability to improve grid strength [10], [11], [12]. Recently, the increasing displacement of synchronous generators (SGs) with GFL and GFM inverter-based apparatuses is shifting the modern power system with high penetration levels of inverter-based apparatuses into a 100% inverter-based power system (IBPS), such as wind farms transmitted by VSC-HVDC system [13], [14]. In such a 100% IBPS, small-signal stability issues may occur due to the interaction between the control loops of GFM and GFL inverters and the interaction between these control loops and the electromagnetic transients of the power network [15].

Understanding under what grid conditions the small-signal stability issues may arise is important for stable and reliable grid operation, especially for 100% IBPSs. The existing methods for the small-signal stability analysis in the large-scale power system with multiple inverters generally fall into two categories, namely time- and frequency-domain methods [16], [17], [18], [19], [20], [21]. The time-domain method is mainly the eigenvalue analysis based on the state-space model, which can represent the dynamic performance of the whole system in detail [16], [17]. However, it is challenging to apply the eigenvalue analysis method to large-scale power systems with high inverter penetration due to the significant obstacles in formulating and analyzing the complete state-space model. With hundreds of inverters in the system and each containing tens of states, it leads to a very high-order system state matrix and thus a high demand for computational power [18]. Also, the inverter control algorithms are usually different from vendors and are usually black-boxed and protected as intellectual property, which further prevents the accurate formulation of the state-space model [19]. On the other hand, frequency-domain impedance methods are suitable for black-boxed inverter models since the impedance model can be measured by external frequency scanning without disclosing inverter details [19], [20], [21]. Although the existing impedance methods can precisely give small-signal stability assessment results [21], they rely on the impedance spectral of all elements in the system (such as all line impedance), which leads to a high computational demand since it needs scanning

0885-8977 © 2024 IEEE. Personal use is permitted, but republication/redistribution requires IEEE permission. See https://www.ieee.org/publications/rights/index.html for more information.

hundreds of frequency points. Also, compressing the whole system into a single impedance [21] or impedance ratio [20] for the stability evaluation (such as Nyquist criterion) may lead to a loss of connection with the original system [18], so the existing impedance methods are not interpretive in relating instability issues back to physical nature in real power systems.

Therefore, grid strength assessment is often used to fast identify the weak grid areas where the small-signal stability issues may occur and then determine if more detailed analyses are required. The concept of small-signal grid strength is introduced to relate the grid strength with the small-signal stability issues [7]. Note that this paper focuses on the grid strength in terms of small-signal stability analysis. Various indices have been developed for quantifying the grid strength in the literature. Short-circuit ratio (SCR) is the most common one [19], [22], but it cannot consider the impact of interaction between IBRs on grid strength. To address this shortcoming, various indices are proposed such as the weighted SCR (WSCR) [24], the composite SCR (CSCR) [25], the equivalent SCR (ESCR) [26], and the SCR with interaction factors (SCRIF) [27]. These indices may lack the theoretical justification for the relationship between grid strength and small-signal stability. Moreover, the thresholds required for these indices to identify the small-signal stability are defined based on either empirical reasoning or electromagnetic transient simulations based on trial and error, which also lack theoretical explanation and thus may lead to conservative or even misleading results to assess grid strength in terms of the small-signal stability. These two concerns are addressed by the generalized SCR (gSCR) [28].

However, these existing methods cannot be used for a 100% IBPS dominated by both GFL and GFM inverters to assess smallsignal stability analysis from the perspective of grid strength, due to the following challenges: 1) It is not clear the impact of voltage characteristics of GFM inverters on voltage support capability in the 100% IBPS dominated by both GFL and GFM inverters. The 100% IBPS is different from a power system dominated by GFL inverters. The former does not have synchronous generators to provide voltage support while the latter does. While GFM inverters can provide voltage support in the 100% IBPS, it remains unclear how GFM inverters affect grid strength. 2) It remains unclear the oscillation mechanism resulting from the dynamic interaction among GFM and GFL inverters in such a 100% IBPS. The mechanism analysis becomes complex when there are many inverters in a 100% IBPS due to the complicated interaction of inverter controls. 3) It is also unclear the relationship between grid strength and the small-signal stability in such a 100% IBPS.

By addressing these challenges, this paper presents a method for quickly identifying the small-signal stability issues in a 100% IBPS from the perspective of grid strength. The major contributions of the paper include:

1) We analyze the voltage characteristics of GFM inverters and reveal how to model the impact of GFM inverters on grid strength. On this basis, we form a multi-inverter system modeling for a 100% IBPS and transform it into a set of simple subsystems to analyze the small-signal stability driven by the dynamic interaction among GFM and GFL inverters while reducing the complexity of analysis due to the interaction in a power system with many inverters.

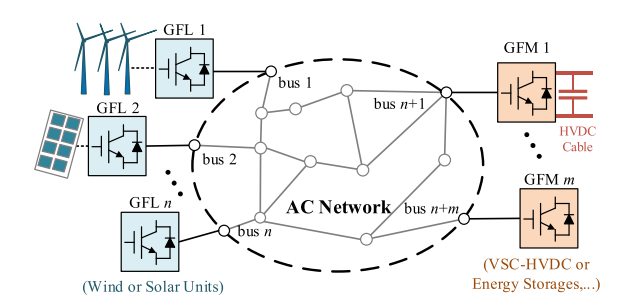


Fig. 1. Illustration of a 100% IBPS.

- 2) We develop an index and its threshold to interpret small-signal stability issues from the perspective of grid strength. The proposed index includes the impact of voltage support characteristics of GFM inverters on grid strength assessment, and it is formulated from the characteristics of the original network topology and parameters in the 100% IBPS. The threshold of the proposed index reflects the lowest grid strength of the system in terms of the small-signal stability boundary, and it can be quickly determined without the need for electromagnetic transient simulations based on trial and error.
- 3) Based on the proposed index and its threshold, we propose a rapid pre-screening method for identifying the potential small-signal oscillation instability issues and quantifying the small-signal stability margin in the 100% IBPS based on the grid strength assessment. The proposed method is implemented based on the fundamental-frequency network admittance and grey- and black-boxed models of inverters, instead of formulating very high-order state matrix or frequency screening of all elements in the system.

The rest of this paper is organized as follows. Section II discusses challenges to grid strength assessment in the 100% IBPS dominated by GFM and GFL inverters. In Section III, the frequency-domain admittance model for a typical GFM inverter is derived to analyze its voltage support characteristics. In Section IV, we develop a multi-inverter system modeling for the 100% IBPS by integrating the GFM inverter models with the models for GFM inverters and the power network. In Section V, the heterogenous multi-inverter system is transformed into a set of subsystems for the small-signal stability analysis. In Section VI, we propose an index and its threshold to quantify grid strength and develop a method for grid strength assessment in terms of small-signal stability. The proposed method is validated in Section VII. The conclusions are drawn in Section VIII.

II. PROBLEM STATEMENT

With the large-scale renewable integration, 100% IBPSs are emerging. Fig. 1 illustrates a typical 100% IBPS, where the renewable resources such as wind and solar resources are integrated into the power system via GFL inverters, and the renewable power is delivered from the system to the external grid via VSC-HVDC [4]. The VSC-HVDC and other apparatuses such as energy storages are interfaced with the system via GFM inverters to provide voltage support [11].

For such a 100% IBPS, it is important to understand and identify the small-signal stability issues caused by the interaction between the control loops of GFM and GFL inverters and the interaction between these control loops and the electromagnetic transients of the power network. Grid strength assessment is often used to fast identify the weak grid areas where small-signal stability issues may occur and then determine if more detailed analyses are required. Various metrics have been developed to quantify the grid strength. Since most of these existing metrics are developed based on the concept of SCR, we take the SCR as an example to discuss the major challenges for assessing the grid strength in terms of the small-signal stability in a 100% IBPS with GFL and GFM inverters. The SCR is defined as the ratio of the short circuit capacity S_{POI} at a point of interconnection (POI) for an inverter to the rated capacity S_B of the inverter [28]

$$SCR = \frac{S_{POI}}{S_B} = \frac{U_N^2/Z}{S_B} = \frac{1}{S_B Z} = \frac{B}{S_B}$$
 (1)

where $U_{\rm N}=1.0$ p.u. represents the rated voltage at the POI; Z=1/B is the Thevenin reactance evaluated based on network reactance; B represents the network susceptance in the single-inverter-based system.

Based on the SCR defined in (1), there are the following challenges of assessing grid strength in terms of the small-signal stability in a 100% IBPS with GFL and GFM inverters.

- 1) In the concept of SCR, the network reactance is used to quantify grid strength for reflecting the sensitivity of the voltage at a POI for an GFL inverter to the inverter current injection [26]. When SCR is smaller (i.e., the network impedance is larger), the voltage is more sensitive to the GFL inverter and thus causes small-signal stability issues. However, in the 100% IBPS dominated by GFM and GFL inverters, it remains unclear how GFM inverter nature is included in the network impedance to define indices for grid strength assessment.
- 2) To assess small-signal stability from the perspective of grid strength, it is required to analyze the small-signal stability in the 100% IBPS. However, when such an IBPS has many GFM and GFL inverters, the analysis is challenging due to the complex interaction between the control loops of GFM and GFL inverters and the interaction between these control loops and the electromagnetic transients of the power network.
- 3) To identify the small-signal stability issues by grid strength assessment, it needs to understand the relationship between grid strength and the small-signal stability in such a 100% IBPS. Particularly, it needs to determine a threshold for SCR. For example, when a POI has a threshold for SCR less than 3, the small-signal stability is likely to occur at the POI [26]. However, such a threshold changes with system conditions such as network topologies, the number of connected inverters, their capacities, etc. The threshold is commonly derived by empirical reasoning or electromagnetic transient simulations based on trial and error. It is challenging to determine such a threshold to characterize the system stability boundary in the 100% IBPS dominated by GFM and GFL inverters.

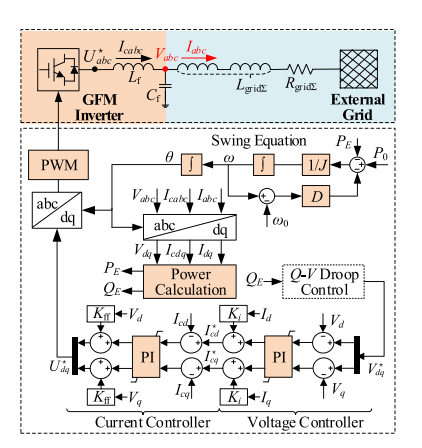


Fig. 2. Scheme of a GFM inverter based on a normal virtual synchronous machine control

In the following sections, we will address the challenges and propose a method for fast assessing grid strength in terms of the small-signal stability in the 100% IBPS.

III. VOLTAGE SUPPORT CHARACTERISTIC ANALYSIS OF GRID-FORMING INVERTERS

To model the 100% IBPS as a multi-inverter system in the next section, this section will formulate the frequency-domain admittance modeling for a GFM inverter to analyze its voltage support characteristics.

A. Admittance Modeling for GFM Inverters

According to [29], it is known that the virtual synchronous machine control scheme can be equivalent to other GFM control schemes. Without loss of generality, we will derive the frequency-domain admittance modeling for GFM inverter with the virtual synchronous machine control structure shown in Fig. 2. In Fig. 2, a three-phase GFM inverter is linked to the external grid through an LCL-type filter (LCL refers to inductance(L)-capacitance(C)-inductance(L)), where V_{abc} is the three-phase terminal voltage of the capacitor, I_{cabc} is the current of inverter-side filter inductance, and I_{abc} is the output current injected into the ac grid. The voltages and currents are represented in the local dq-frame due to GFM control blocks. V_{abc} and I_{cabc} are measured as feedback control variables of the vector control based on Park transformation. The angular frequency of the dq-axis ω for Park transformation is governed by the swing equation. To facilitate this derivation, the voltage and current will be represented in terms of complex space vectors (e.g., $\dot{V} = V_d + jV_q$ represents the complex space vector of V_{abc}). The admittance model in the frequency domain (i.e., s-domain) can be derived for the GFM inverter based on the voltage and currents at the inverter side. The detailed derivation is presented as follows.

The terminal voltage \vec{U} and its reference \vec{U}^* at the inverter side can be formulated in the complex space vector frame [10]

$$\vec{U} = \vec{V} + (sL_f + j\omega L_f)\vec{I_c} \tag{2}$$

$$\vec{U}^{\star} = K_{\rm ff}(s)\vec{V} + G_i(s)(\vec{I}_c^{\star} - \vec{I}_c)$$
 (3)

$$\vec{I}_c = (sC_f + j\omega C_f)\vec{V} + \vec{I} \tag{4}$$

$$\vec{I}_c^{\star} = G_v(s)(\vec{V}^{\star} - \vec{V}) + j\omega C_f \vec{V} + K_i \vec{I}$$
 (5)

where \vec{I}_c and \vec{I}_c^{\star} represent the inverter filter current and its reference; $L_{\rm f}$ represents the filter inductance; $C_{\rm f}$ represents the filter capacitor; $G_i(s) = K_{pi} + K_{ii}/s$ represents the transfer functions of the current feedback PI controller, with K_{pi} and Kii being the proportion and integral coefficients of the current PI controller; $K_{\rm ff}(s) = 1/(1 + T_{\rm vf}s)$ represents the transfer function of the terminal voltage feed-forward low-pass filter; $G_v(s) = K_{pv} + K_{iv}/s$ represents the transfer function of the voltage feedback PI controller, with $K_{\rm pv}$ and $K_{\rm iv}$ being the proportion and integral coefficients of the voltage PI controller; K_i represents the current feed-forward efficient; \vec{V}^* is the reference of the terminal voltage \vec{V} . It should be noted that $\vec{U} \approx \vec{U}^{\star}$ when neglecting PWM time delay, which does not affect oscillation instability within the bandwidth frequency of PLL [19]; $\Delta \vec{V}^{\star} = 0$ (i.e., the constant voltage reference) when the Q-V droop controller is not considered.

By combining (2)–(5), a Thevenin equivalent circuit equation can be formed as

$$K_V(s)\vec{V}^* - \vec{V} = Y_o^{-1}(s)\vec{I}$$
 (6)

$$Y_o(s) = \frac{G_v(s)H_I(s) - H_{FF}(s) + sC_f + j\omega C_f[1 - H_I(s)]}{1 - K_iH_I(s)},$$

$$K_{V}(s) = \frac{H_{I}(s)G_{v}(s)}{G_{v}(s)H_{I}(s) - H_{FF}(s) + sC_{f} + j\omega C_{f}[1 - H_{I}(s)]},$$

$$H_I(s) = \frac{G_i(s)}{G_i(s) + sL_f + j\omega L_f}, H_{FF}(s) \frac{1 - K_{ff}(s)}{G_i(s) + sL_f + j\omega L_f}$$
(7)

In (6), $K_V(s)\vec{V}^*$ can be viewed as a voltage source under a small signal due to $\Delta \vec{V}^* = 0$.

By linearizing (6), we have the admittance model $Y_o(s)$ for the GFM inverter

$$-\Delta \vec{I} = Y_o(s)\Delta \vec{V} \tag{8}$$

where the symbol Δ represents the change of variable or vector under the small signal scenario.

In (8), the admittance model $Y_o(s)$ can further be simplified. The transfer function of the voltage feedforward low-pass filter satisfies $[1-K_{\rm ff}(s)]\approx 0$ [6]; Also, the current feed-forward coefficient meets $K_i=1$. Thus, $Y_o(s)$ can be rewritten as

$$Y_o(s) = Y_L(s) + Y_C(s) \tag{9}$$

$$Y_L(s) = \frac{H_V(s)}{L_f(s+j\omega)}, Y_C(s) = C_f(s+j\omega)$$
 (10)

where $Y_L(s)$ is an equivalent inductive susceptance under control; $Y_C(s)$ is a pure capacitive susceptance of the filter; and $H_V(s) = G_i(s)[sC_{\rm f} + G_v(s)]$ is a transfer function containing the transfer functions of voltage and current PI regulator.

In (9), $Y_C(s)$ can be further neglected since the impact of shunt filter capacitor C_f is mainly manifested in the high frequency band (>100 Hz) and has little correlation with the oscillation

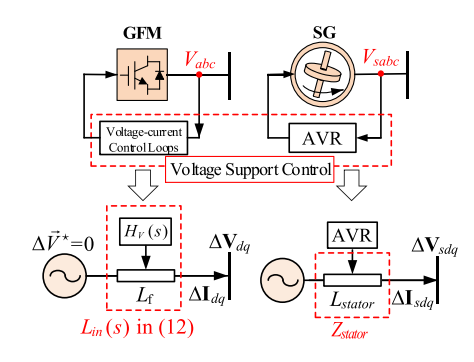


Fig. 3. Illustration of voltage support characteristics of a GFM inverter analogous to a SG based on similar voltage-feedback control structure and circuit modeling.

instability within the bandwidth frequency of PLL that we focus on [19]. According to [10], the admittance model $Y_o(s)$ in (8) can be rewritten in the following transfer matrix form $\mathbf{Y}_{dq}(s)$ by transforming current and voltage vectors from complex space to the dq-frame.

$$-\Delta \mathbf{I}_{dq} = \mathbf{Y}_{dq}(s)\Delta \mathbf{V}_{dq} \tag{11}$$

$$\mathbf{Y}_{dq}(s) \approx \frac{1}{\omega_0 L_{in}(s)} \mathbf{F}(s)$$
 (12)

$$L_{in}(s) = \frac{1}{H_V(s)} L_f \tag{13}$$

$$\mathbf{F}(s) = \begin{bmatrix} \beta(s) & \alpha(s) \\ -\alpha(s) & \beta(s) \end{bmatrix}$$
 (14)

where $\Delta \mathbf{I}_{dq} = [\Delta I_d, \Delta I_q]^{\top}$ and $\Delta \mathbf{V}_{dq} = [\Delta V_d, \Delta V_q]^{\top}$ represent the perturbed vectors of the injected current and terminal voltage of an inverter in the dq reference frame, respectively; $\beta(s) = s\omega_0/(s^2 + \omega_0^2)$ and $\alpha(s) = \omega_0^2/(s^2 + \omega_0^2)$ are the elements of the transfer function matrix form; $\omega_0 = 2\pi f_0 = 100\pi rad/s$ represents the angular fundamental frequency. $\mathbf{Y}_{dq}(s)$ represents the admittance model for the GFM inverter in the dq reference frame. $L_{in}(s)$ represents a transfer function integrated with voltage and current control dynamics in $H_V(s) = G_i(s)[sC_f + G_v(s)]$.

B. Voltage Support Characteristics of GFM Inverters

In (11), the admittance model $\mathbf{Y}_{dq}(s)$ for the GFM inverter reveals its voltage support function analogous to a SG as shown in Fig. 3. It is well known that a SG can be represented by a voltage source in series with a synchronous reactance Z_{stator} (or a synchronous inductance L_{stator}) based on the constant flux linkage model. The synchronous inductance can be affected by the automatic voltage regulator (AVR) to change flux linkage to control the terminal voltage [22]. Thus, the voltage support capability of the SG can be adjusted by the AVR. In (12), the admittance model $\mathbf{Y}_{dq}(s)$ for the GFM inverter has a similar voltage support capability to the SG since the frequency-domain inductance $L_{in}(s)$ within $\mathbf{Y}_{dq}(s)$ can be adjusted by a transfer function $H_V(s)$, as shown in (13). Thus, $L_{in}(s)$ can be viewed

TABLE I Variation Parameters of Voltage and Current Regulator in Four Different Test Cases

Case	PI Parameters of $G_{\nu}(s)$	PI Parameters of $G_i(s)$
1	$K_{pv} = 2$, $K_{iv} = 30$	$K_{pi} = 0.3, K_{ii} = 10$
2	$K_{pv} = 2.13, K_{iv} = 10$	$K_{pi} = 0.3, K_{ii} = 12$
3	$K_{pv} = 2.5, K_{iv} = 50$	$K_{pi} = 0.32, K_{ii} = 20$
4	$K_{pv} = 3, K_{iv} = 40$	$K_{pi} = 0.4, K_{ii} = 30$

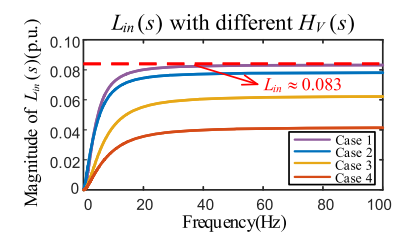


Fig. 4. Frequency response change of inductance $L_{in}(s)$ with the transfer function $H_V(s)$ under different voltage-current control parameters listed in Table I.

as the internal equivalent inductance for the GFM inverter, which is analogous to the synchronous inductance for the SG.

To illustrate the change of the inductance $L_{in}(s)$ with the transfer function $H_V(s)$, let us consider a grid-connected GFM inverter system in Fig. 2. The used inverter parameters are presented in Table IV of Appendix A. Fig. 4 shows the frequency response change of $L_{in}(s)$ with transfer function $H_V(s)$ under different voltage-current control parameters listed in Table I. Fig. 4 shows that $L_{in}(s)$ changes with $H_V(s)$ due to various inverter control parameters for $G_i(s)$ and $G_v(s)$. It can be observed from this figure that for given inverter control parameters, the value of $L_{in}(s)$ almost remains constant within the wide range of the frequency band we are concerned. For example, in Fig. 4, $L_{in}(s)$ in Case 1 almost keep a constant around 0.083 p.u. within the frequency band from 10 to 100 Hz.

According to the observation, the value of $L_{in}(s)$ in (12) can be approximated by a constant L_{in} for given inverter control parameters, when the sideband oscillations of fundamental frequency (f_0) is considered for small-signal stability analysis [19]. Due to the relationship between $L_{in}(s)$ and $H_V(s)$ in (13), the constant L_{in} can be adjusted by tuning the parameters in $H_V(s)$. Thus, $\mathbf{Y}_{dq}(s)$ for the GFM inverter in (12) can be rewritten

$$\mathbf{Y}_{dq}(s) \approx \frac{1}{\omega_0 L_{in}} \mathbf{F}(s)$$
 (15)

IV. Modeling of 100% Inverter-based Power Systems

With the modeling for GFM inverters constructed in Section III, we will use the frequency-domain admittance modeling to formulate a heterogenous multi-inverter system for the 100% IBPS as shown in Fig. 1. Such a 100% IBPS contains n different GFL inverters (connected buses $1 \sim n$), m different GFM inverters (connected buses $n+1 \sim n+m$) and interior buses without any directly connected inverters. The assumptions in [28] are used for simplifying the analysis and all the loads are simple constant current loads that play no role for the small-signal admittance modeling. The multi-inverter system is

formulated by integrating the inverter model with the power network model.

A. Inverter Modeling

For either GFL or GFM inverters, their output currents and voltages are commonly represented in the local dq reference frame due to their inverter control blocks. To facilitate the integration of inverter model with the power network model to construct the model for the system shown in Fig. 1, the components of the output currents and voltage for each inverter represented in the local dq frame will be transformed into their corresponding components in the global xy reference frame using (16), which is derived based on the relationship between the local and global reference frames,

$$\Delta \mathbf{I}_{dqk} = \Delta \mathbf{I}_{xyk} + \mathbf{I}_{0k} \Delta \theta_k, \Delta \mathbf{V}_{dqk} = \Delta \mathbf{V}_{xyk} + \mathbf{V}_{0k} \Delta \theta_k.$$
 (16)

where $\Delta\theta_k$ is the angle between the local dq reference frame and the global xy reference frame for the k-th inverter $(k=1,\ldots,n+m)$; $\Delta\mathbf{I}_{xyk}=[\Delta I_{xk},\Delta I_{yk}]^{\top}$ and $\Delta\mathbf{V}_{xyk}=[\Delta V_{xk},\Delta V_{yk}]^{\top}$ are the vectors of the output current and terminal voltage of the k-th inverter in the x-axis and y-axis reference frame; $\mathbf{I}_{0k}=[I_{q0k},-I_{d0k}]^{\top}$ and $\mathbf{V}_{0k}=[V_{q0k},-V_{d0k}]^{\top}$ are the vectors of the output current and terminal voltage of the k-th inverter in the local dq reference frame before disturbances. The detailed derivation of (16) can be found in [30].

1) *GFL Inverter Modeling:* In the literature, different admittance models in the frequency domain have been proposed for GFL inverters. In this paper, we will use the one in [31] for modeling *n* GFL inverters, which can be generally represented by

$$\Delta \mathbf{I}_{xvi} = S_{bi} \mathbf{Y}_{GFL,i}(s) \Delta \mathbf{V}_{xvi}, i = 1, \dots, n$$
 (17)

where $\mathbf{Y}_{GFL,i}(s)$ is the admittance matrix for the *i*-th GFL inverter in the global xy reference frame $(i=1,\ldots,n)$; S_{bi} denotes the ratio of capacity of the *i*-th GFL inverter to the base capacity of the system. Since all GFL inverters have different control parameters and capacities, their $\mathbf{Y}_{GFL,i}(s)$ and S_{bi} are different.

2) GFM Inverter Modeling: To transform the admittance model of GFM inverters derived in Section III in the local dq reference frame into the one in the global xy reference frame, we first represent the change of angle θ in (16) by (18):

$$\Delta\theta = -\frac{F_P(s)}{Js^2 + Ds} \Delta P_E \tag{18}$$

where $F_P(s) = k_P/(1 + T_P s)$ is the normal first-order lowpass filter for power measurement; J and D are the inertia and damping coefficient of the swing equation respectively; and P_E is the active power tied with the angular frequency.

By combining (11) and (16) with (18), the admittance model for the *j*-th GFM inverter in the global *xy* reference frame can be represented by (19) and (20), and the detailed derivation of (19) and (20) can be found in Appendix B

$$\Delta \mathbf{I}_{xyj} = S_{bm,j} \mathbf{Y}_{GFM,j}(s) \Delta \mathbf{V}_{xyj} j = 1, \dots, m$$
 (19)

$$-\mathbf{Y}_{GFM,j}(s) = \mathbf{Y}_{dq,j}(s) + \mathbf{Y}_{\delta,j}(s)$$
 (20)

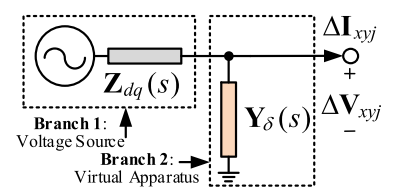


Fig. 5. Illustration of the GFM inverter model in the global xy reference frame.

where $\mathbf{Y}_{GFM,j}(s)$ is the admittance matrix for the *j*-th GFM inverter represented in the global xy reference frame (j=1,...,m); $S_{bm,j}$ denotes the ratio of capacity of the *j*-th GFM inverter to the base capacity of the system. Since all GFM inverters have different control parameters and capacities, their $\mathbf{Y}_{GFM,j}(s)$ and S_{bj} are different.

Equation (20) shows that the model of each GFM inverter in the global xy reference frame consists of two parts, which are illustrated in Fig. 5. The first part can be considered as an equivalent Thevenin circuit representing the voltage source branch, consisting of a grounded voltage source in series with its internal impedance $\mathbf{Z}_{dq}(s) = \mathbf{Y}^{-1}{}_{dq}(s)$, which has been derived by (15) in the local dq reference frame. The second part is a virtual apparatus branch in Fig. 5, which represents the shunt admittance model $\mathbf{Y}_{\delta}(s)$ to include the angle dynamics governed by the swing equation in (18). As a result, the GFM inverter modeling in Fig. 5 offers a modular perspective for analyzing the impact of GFM inverters in 100% IBPS.

B. Power Network Modeling

The power network can be modeled as a frequency-domain admittance matrix where inverter buses are reserved and the other interior buses are eliminated by Kron reduction [28],

$$\Delta \mathbf{I}_{Gxy} = \mathbf{B} \otimes \mathbf{F}(s) \Delta \mathbf{V}_{Gxy} \tag{21}$$

where $\Delta \mathbf{I}_{Gxy} = [\Delta \mathbf{I}_{xy1}, \dots, \Delta \mathbf{I}_{xy,n+m}]^{\top}$ and $\Delta \mathbf{V}_{Gxy} = [\Delta \mathbf{V}_{xy1}, \dots, \Delta \mathbf{V}_{xy,n+m}]^{\top}$ represent the vectors of the currents and terminal voltages of n+m inverters in the xy reference frame; the bold $\mathbf{B} \in \mathbb{R}^{(n+m)\times(n+m)}$ represents the fundamental-frequency node susceptance matrix of the power network of the 100% IBPS; \otimes denotes the Kronecker product.

In (21), matrix $\bf B$ can be modified as a grounded Laplacian matrix $\bf B_{\rm mod}$ by including the voltage source branch for each GFM inverter, as illustrated in Fig. 5. Thus, the modified node susceptance matrix $\bf B_{\rm mod}$ can be obtained by adding the constant internal equivalent inductance of the GFM inverter (i.e., L_{in} in (15)) to the submatrix $\bf B_4$ of matrix $\bf B$:

$$\mathbf{B}_{\text{mod}} = \begin{bmatrix} \mathbf{B}_1 & \mathbf{B}_2 \\ \mathbf{B}_3 & \tilde{\mathbf{B}}_4 \end{bmatrix} \tag{22}$$

$$\tilde{\mathbf{B}}_4 = \mathbf{B}_4 + \mathbf{B}_{in} \tag{23}$$

$$\mathbf{B}_{\mathsf{in}} = diag\{S_{bm,i}B_{in,i}\}\tag{24}$$

where $\mathbf{B}_1 \in \mathbb{R}^{n \times n}$, $\mathbf{B}_2 \in \mathbb{R}^{n \times m}$, $\mathbf{B}_3 = \mathbf{B}_2^{\top} \in \mathbb{R}^{m \times n}$ and $\mathbf{B}_4 \in \mathbb{R}^{m \times m}$ are the submatrices of the matrix \mathbf{B} ; \mathbf{B}_{in} represents a diagonal matrix whose each diagonal element $B_{in,j} = 1/(\omega_0 L_{in,j})$ is the reciprocal of the internal equivalent inductance L_{in} of each

GFM inverter (j = 1, ..., m); $\tilde{\mathbf{B}}_4$ denotes the modified submatrix \mathbf{B}_4 of matrix \mathbf{B} .

C. Heterogeneous Multi-Inverter System for 100% IBPS Modeling

Based on the GFL and GFM inverter modeling in (17) and in (19) as well as the network modeling ${\bf B}$ in (21), the 100% IBPS can be modeled as a closed-loop multi-inverter system. The characteristic equation of the closed-loop heterogenous multi-inverter system can be represented

$$\det \left\{ -\mathbf{Y}_G(s) + \mathbf{B} \otimes \mathbf{F}(s) \right\} = 0 \tag{25}$$

$$\mathbf{Y}_{G}(s) = \begin{bmatrix} diag\{S_{bi}\mathbf{Y}_{GFL,i}(s)\} \\ diag\{S_{bm,j}\mathbf{Y}_{GFM,j}(s)\} \end{bmatrix}$$
(26)

where $\mathbf{Y}_G(s)$ represents the admittance matrix of all n+m inverters.

Equation (25) can also be rewritten as (27) below when replacing matrix \mathbf{B} in (21) with \mathbf{B}_{mod} in (22) to move the voltage source branch for each GFM inverter (as illustrated in Fig. 5) from matrix $\mathbf{Y}_G(s)$ in (26) to \mathbf{B} in (21).

$$\det \left\{ \begin{bmatrix} -diag\{S_{bi}\mathbf{Y}_{GFL,i}(s)\} \\ diag\{S_{bm,j}\mathbf{Y}_{\delta,j}(s)\} \end{bmatrix} + \mathbf{B}_{mod} \otimes \mathbf{F}(s) \right\} = 0$$
(27)

V. SMALL-SIGNAL STABILITY ANALYSIS OF 100% IBPS

By employing the characteristic equation in (27), we can analyze the small-signal stability of the 100% IBPS. However, such analysis is challenging due to the complex interaction between the power network and different GFL and GFM inverters. To reduce the analysis complexity, we will transform the heterogenous multi-inverter system into a set of equivalent subsystems. First, we will formulate a nominal multi-inverter system for the heterogenous multi-inverter system. Then, we will transform the nominal multi-inverter system into a set of subsystems and use the perturbation technique for the small-signal stability analysis of the 100% IBPS.

A. Formulating Nominal Multi-Inverter System

To formulate the nominal multi-inverter system, we first rewrite the characteristic equation in (27) as,

$$0 = \det\{\boldsymbol{M}(s) + \boldsymbol{N}(s)\}\tag{28}$$

$$M(s) = \mathbf{S}_h^{-1}(\mathbf{B}_1 - \mathbf{B}_2\tilde{\mathbf{B}}_4^{-1}\mathbf{B}_2^{\top}) \otimes \mathbf{I}_2$$

$$-diag\{\mathbf{F}^{-1}\mathbf{Y}_{GFL,i}(s)\}\tag{29}$$

$$\mathbf{N}(s) = -\mathbf{S}_b^{-1}(\mathbf{B}_2 \otimes \mathbf{I}_2) \Delta(s) (\mathbf{B}_2^{\top} \otimes \mathbf{I}_2)$$
 (30)

$$\Delta(s) = -\left[\mathbf{I}_{2m} + (\tilde{\mathbf{B}}_{4}^{-1} \otimes \mathbf{I}_{2})diag\{S_{bm,j}\mathbf{F}^{-1}\mathbf{Y}_{\delta,j}(s)\}\right]^{-1}$$
$$(\tilde{\mathbf{B}}_{4}^{-1} \otimes \mathbf{I}_{2}) \cdot diag\{S_{bm,j}\mathbf{F}^{-1}\mathbf{Y}_{\delta,j}(s)\}(\tilde{\mathbf{B}}_{4}^{-1} \otimes \mathbf{I}_{2})$$
(31)

where $\mathbf{S}_b = \operatorname{diag}\{S_{bi}\} \in \mathbb{R}^{n \times n}$ is a diagonal matrix whose each diagonal element is S_{bi} defined in (17). The detailed derivation of (28)–(31) is presented in Appendix C.

Then, we formulate the nominal multi-inverter system based on (28)–(31). Equations (28)–(31) show that the small-signal stability of the 100% IBPS depends on M(s) and N(s). M(s) is relevant to n different GFL inverters and m different GFM inverters interconnected through the power network, and each of these m GFM inverters just has its voltage source branch, which is embedded into the power network via matrix $\tilde{\mathbf{B}}_4$. N(s) has the virtual apparatus branches of all m GFM inverters. We formulate the nominal multi-inverter system based on M(s), and its characteristic equation can be represented

$$\det\{\boldsymbol{M}(s)\}$$

$$= \det\{\mathbf{S}_{b}^{-1}(\mathbf{B}_{1} - \mathbf{B}_{2}\tilde{\mathbf{B}}_{4}^{-1}\mathbf{B}_{2}^{\top}) \otimes \mathbf{I}_{2}$$

$$-diag\{\mathbf{F}^{-1}\mathbf{Y}_{GFL,i}(s)\}\}$$

$$= \det\{(\mathbf{B}_{1} - \mathbf{B}_{2}\tilde{\mathbf{B}}_{4}^{-1}\mathbf{B}_{2}^{\top}) \otimes \mathbf{F}(s)$$

$$-diag\{S_{bi}\mathbf{Y}_{GFL,i}(s)\}\}$$

$$= \det\{-diag\{\mathbf{Y}_{GFL,i}(s)\} + \mathbf{Y}_{eq} \otimes \mathbf{F}(s)\} = 0 \quad (32)$$

$$\mathbf{Y}_{eq} = \mathbf{S}_{b}^{-1}(\mathbf{B}_{1} - \mathbf{B}_{2}\tilde{\mathbf{B}}_{4}^{-1}\mathbf{B}_{2}^{\top}) \quad (33)$$

where $Y_{\rm eq}$ is a weighted and grounded Laplacian matrix [31] for the equivalent power network that considers the equivalent voltage source branches of GFM inverters.

B. Small-signal Stability Analysis Based on Nominal Multi-Inverter Systems

Based on the nominal multi-inverter system in (32), we will analyze the small-signal stability of the heterogenous multi-inverter system for the 100% IBPS by using the matrix perturbation technique. In the nominal multi-inverter system, each of m different GFM inverters is just modeled by the voltage source branch of the GFM inverter as illustrated in Fig. 5. To include the virtual apparatus branch for each GFM inverter in the nominal multi-inverter system for the small-signal stability analysis, we will use the perturbation technique to treat the impact of the virtual apparatus branches of all m different GFM inverters as the additive perturbation to the small-signal stability of this nominal multi-inverter system.

According to [35], the nominal multi-inverter system in (32) is a heterogeneous one, where the power network connects all *n* different GFL inverters to *m* equivalent voltage sources, representing *m* GFM inverters in (19) with their voltage source branches embedded in the power network. Such a heterogeneous system can be transformed into a set of equivalent single-inverter subsystems based on the modal decoupling method for the small-signal analysis [35], and the stability of the entire system depends on the most critical subsystem when the control configuration and parameters of all *n* different GFL inverters are given. In other words, each decoupled subsystem has some of these modes of the entire nominal system in (32), and particularly, the most critical subsystem has the system dominant modes. The characteristic equation of the most critical subsystem can

be represented by

$$\det\{\lambda_1 \mathbf{I}_2 - \sum_{i=1}^n p_{1i} \mathbf{F}^{-1} \mathbf{Y}_{GFL,i}(s)\} = 0$$
 (34)

where λ_1 is the smallest eigenvalue of the matrix \mathbf{Y}_{eq} in (32); $p_{1i} = v_{1i}u_{1i}$ represents the participation factor of the smallest eigenvalue (i = 1, ..., n); v_{1i} and u_{1i} are the *i*-th elements of the vectors v_1 and u_1 , respectively; v_1 and u_1 are the left and right normalized eigenvectors corresponding to the smallest eigenvalue λ_1 and they satisfy $v_1^T u_1 = 1$.

Since the small-signal stability of the nominal multi-inverter system depends on its most critical subsystem in (34), the perturbation to the small-signal stability of the nominal multi-inverter system is the one to the stability of the most critical subsystem. The perturbed subsystem can be represented by

$$\det\{\lambda_1 \mathbf{I}_2 - \sum_{i=1}^n p_{1i} \mathbf{F}^{-1} \mathbf{Y}_{GFL,i}(s) + \delta_{GFM}(s)\} = 0 \quad (35)$$

where $\delta_{GFM}(s) = [v_1 \otimes \mathbf{I}_2]^{\top} N(s) [u_1 \otimes \mathbf{I}_2]$ denotes the perturbation from the virtual apparatus branches of all m different GFM inverters.

The following Lemma 1 proves that the small-signal stability of the system in (28) can be approximately characterized by the perturbed subsystem in (35).

Definition 1: The eigenvalues of a transfer function matrix such as G(s) can be expressed as a function regarding the variable s, and the eigenvalues of matrix G(s) are defined as the eigenvalue function of G(s) about variable s. The eigenvalue function of G(s) corresponding to its dominant eigenvalue is defined as the dominant eigenvalue function of G(s).

Lemma 1: Define μ and $\bar{\mu}$ as the dominant eigenvalue function of the 100% IBPS in (28) and the perturbed subsystem in (35), respectively, which are pertinent to the system's dominant eigenvalues. Then, μ and $\bar{\mu}$ have the relationship:

$$\mu = \bar{\mu} + o(\|\mathbf{N}(s)\|) \tag{36}$$

Where $o(\cdot)$ is the second-order and much higher-order approximate error of a function; $\|\cdot\|$ is the norm of the matrix.

Proof: The dominant eigenvalue function $\bar{\mu}$ of the perturbed subsystem in (35) can be represented by

$$\bar{\mu} = \lambda_1 \mathbf{I}_2 - \sum_{i=1}^n p_{1i} \mathbf{F}^{-1} \mathbf{Y}_{GFL,i}(s) + \delta_{GFM}(s)$$
 (37)

By matrix perturbation theory (Theorem 2.3 in [32]), we consider the orignal heterogenoues multi-inverter system for the 100% IBPS as the perturbed nominal multi-inverter system. Since the small-signal stability of the nominal multi-inverter system depends on the most critical subsystem, the dominant eigenvalue function μ for the 100% IBPS is given as:

$$\mu = [v_1 \otimes \mathbf{I}_2]^{\top} \boldsymbol{M}(s) [u_1 \otimes \mathbf{I}_2]$$
$$+ [v_1 \otimes \mathbf{I}_2]^{\top} \boldsymbol{N}(s) [u_1 \otimes \mathbf{I}_2] + o(\|\boldsymbol{N}(s)\|)$$
$$= \lambda_1 \mathbf{I}_2 - \sum_{i=1}^n p_{1i} \mathbf{F}^{-1} \mathbf{Y}_{GFL,i}(s)$$

$$+ [v_1 \otimes \mathbf{I}_2]^{\top} \boldsymbol{N}(s) [u_1 \otimes \mathbf{I}_2] + o(\|\boldsymbol{N}(s)\|)$$

= $\bar{\mu} + o(\|\boldsymbol{N}(s)\|)$ (38)

This concludes the proof.

Based on Lemma 1, the small-signal stability of the 100% IBPS in (28) can be analyzed by the characteristic equation of the most critical subsystem in (35). Equation (35) shows that for the given control strategy and parameters of GFL and GFM inverters, the small-signal stability of the 100% IBPS depends on the smallest eigenvalue λ_1 . It should be noted that λ_1 is not a complex number and is not the mode of the closed-loop system (i.e., the solution of the closed-loop system characteristic equation in (25)). Instead, λ_1 is the smallest eigenvalue of the weighted and grounded Laplacian matrix of the equivalent power network \mathbf{Y}_{eq} (i.e., the proposed grid strength index below).

Furthermore, it is worth noting that the small-signal stability analysis based on the derived most critical subsystem has two main advantages over the traditional analysis approaches (e.g., eigenvalue analysis):

First, the derived most critical subsystem can reduce the analysis complexity of the small-signal stability in a multi-inverter power system by circumventing the formulation and evaluation of a very high-order system state matrix. This lays a foundation for fast pre-screening the small-signal stability issues in a large-scale 100% IBPS with high penetration of GFL and GFM inverters from the perspective of grid strength.

Second, the derived most critical subsystem also facilitates the understanding and assessment of the grid strength of the 100% IBPS based on the concept of the traditional SCR technique. The critical subsystem is an equivalent single-inverter system and can consider the dynamic interaction among GFL and GFM inverters. By levering the analytical results based on this critical subsystem, we will propose the index for grid strength assessment. The index has a similar physical interpretation to that of SCR, thus enabling to extend the existing experience based on the concept of traditional SCR technique to a 100% IBPS for understanding and assessing the small-signal stability from the perspective of grid strength. As a result, an approach based on the proposed index will be developed to quickly identify the potential small-signal stability issues in the 100% IBPS. More details will be presented below.

VI. GRID STRENGTH ASSESSMENT FOR 100% IBPS

According to the analysis results in the previous section, in this section we will define an index for grid strength quantification and derive an analytical expression to determine the index threshold for characterizing the small-signal stability boundary. With the defined index and its threshold, a method will be proposed for assessing grid strength in terms of the small-signal stability and stability margin of the 100% IBPS.

A. Proposed Index for Grid Strength Quantification

As discussed before, the small-signal stability of the 100% IBPS depends on the smallest eigenvalue λ_1 for the given control strategy and parameters of GFL and GFM inverters. Thus, we

define λ_1 as the generalized SCR (gSCR) to quantify grid strength in terms of the small-signal stability in the system.

$$gSCR := \lambda_1 = \min \lambda \{ \mathbf{Y}_{eq} \} = 1/\max \lambda \{ \mathbf{ZS}_b \}$$
 (39)

where $\lambda\{\cdot\}$ denotes eigenvalue solution to a matrix; $\mathbf{Z} = (\mathbf{B}_1 - \mathbf{B}_2 \tilde{\mathbf{B}}_4^{-1} \mathbf{B}_3)^{-1}$ represents the network impedance matrix. The gSCR defined in (39) has the following features:

First, the gSCR essentially reflects the reciprocal of a sensitivity of inverter terminal voltage to inverter current injection in the 100% IBPS. The gSCR is defined based on λ_1 , which is the smallest eigenvalue of admittance matrix \mathbf{Y}_{eq} . Matrix \mathbf{Y}_{eq} reflects the reciprocal of a sensitivity of the terminal voltages at distributed inverters to their inverter current injections in the system. Thus, λ_1 can be viewed as an equivalent netowrk admittance in the most critical subsystem, and it reflects the reciprocal of a sensitivity of the terminal voltage at the equivalent inverter to its current injection.

Second, the gSCR as an equivalent network admittance includes the voltage support characteristics of GFM inverters. As shown in (39), the gSCR is calculated from the admittance matrix $Y_{\rm eq}$ in (33). Matrix $Y_{\rm eq}$ is formulated by embedding the voltage source branch of each GFM inverter into the power network. Thus, the gSCR includes both the network information and voltage support characteristics of GFM. This implies that in the 100% IBPS domianted by GFM and GFL inverters, when only network admittance (or network impedance) is used to define an index to quantify grid strength, this index may not effectively reflect a sensitivity of inverter terminal voltage with respect to inverter current injection.

It should be noted that the gSCR in (39) is different from the one defined in [28]. In [28], the gSCR is defined only based on the network impedance, so it is mainly used for assessing the grid strength of a power system with high penetration of GFL inverters. But the gSCR in (39) is defined based on both network impedance and GFM inverter nature. Thus, the gSCR in (39) is used for grid strength assessment of the 100% IBPS dominated by GFL and GFM inverters.

B. Determining Threshold for Proposed Index

When the gSCR defined in (39) is used to assess grid strength in terms of the small-signal stability in the 100% IBPS, it needs to determine the threshold for characterizing the system stability boundary. The threshold is defined as critical gSCR (CgSCR), which is the value of gSCR calculated under critical operating conditions when the system is critically stable. Thus, CgSCR quantifies the lowest grid strength. If the grid strength quantified by gSCR is smaller than CgSCR, the system loses its small-signal stability.

It should be noted that the thresholds 3, 2 or 1 commonly used for SCR (such as SCR>3) are determined based on the engineering experience in the context of the traditional HVDC-dominated system [36]. These thresholds are not suitable for a power system dominated by GFL and GFM inverters, especially for the 100% IBPS, since such a system has different dynamics from the traditional HVDC-dominated system. In fact, the thresholds of grid strength are changing with power

network topology and apparatuses in a specific power system under different operating conditions, and there are no specific criteria or rules of thumb determining the acceptable threshold [23], [27]. In other words, the commonly used thresholds of the traditional SCR index may lead to the misleading results of identifying the small-signal stability issues in the inverter-based power system [24]. For a power system with the given network topology and IBR control parameters, the threshold is usually determined by electromagnetic transient simulations based on trial and error, which, however, is tedious and computationally challenging.

To tackle this challenge, the threshold CgSCR can quickly be determined based on the analytical expression in the 100% IBPS

$$0 = \det\{gSCR^*\mathbf{I}_2 - \sum_{i=1}^n p_{1i}\mathbf{F}^{-1}\mathbf{Y}_{GFL,i}(s_c) + \delta_{GFM}(s_c)\},$$

$$\begin{cases} CgSCR = gSCR^* \\ Re\{s_c\} = Re\{j\omega_c\} = 0 \end{cases}$$
 (40)

where Re $\{\cdot\}$ denotes the real part of a complex number. $s_c = j\omega_c$ denotes the dominant eigenvalue just located at the imaginary axis in the complex plane, (i.e., system is critically stable); gSCR* is the variable defined as CgSCR related to the critical operating condition.

Equation (40) reveals that the CgSCR characterizing system stability boundary is associated with the power network and the dynamics of both GFL and GFM inverters in the 100% IBPS. Moreover, GFL and GFM inverter dynamics have different impacts on the CgSCR. The GFL inverters influence the CgSCR via the admittance matrix $\mathbf{Y}_{GFL}(s)$, while the GFM inverters affect the CgSCR via the frequecy-domain function $\delta_{GFM}(s)$. This analytical expression of the threshold can provide a potential insight to analyze the impacts of GFL and GFM inverters on the system stability boundary.

C. Proposed Method for Grid Strength Assessment

With the gSCR and CgSCR, we propose a gSCR-based method for assessing small-signal stability and stability margin in the 100% IBPS dominated by GFL and GFM inverters. More specifically, by comparing the gSCR with the proposed CgSCR, the weak grids can be distinguished from strong grids in terms of the small-signal stability in a power system dominated by GFM and GFL inverters. If a grid has gSCR larger than CgSCR (i.e., gSCR≥CgSCR), this grid is strong and will not lose its small-signal stability; otherwise, this grid is weak and will lose its small-signal stability. Furthermore, the stability margin of the 100% IBPS can be assessed by the difference between the proposed gSCR and CgSCR normalized by the CgSCR, as the following equation:

$$\beta\% := \frac{gSCR - CgSCR}{CaSCR} \times 100\% \tag{41}$$

where $\beta\%$ represents the normalized stability margin indicator. The proposed $\beta\%$ in (41) allows one to ensure the sufficiency of system stability margin when $\beta\%$ is larger than a given number such as $\beta_0\%$ (i.e., $\beta\% \geq \beta_0\%$). $\beta_0\%$ can be decided by grid planners and operators based on engineering experience for a

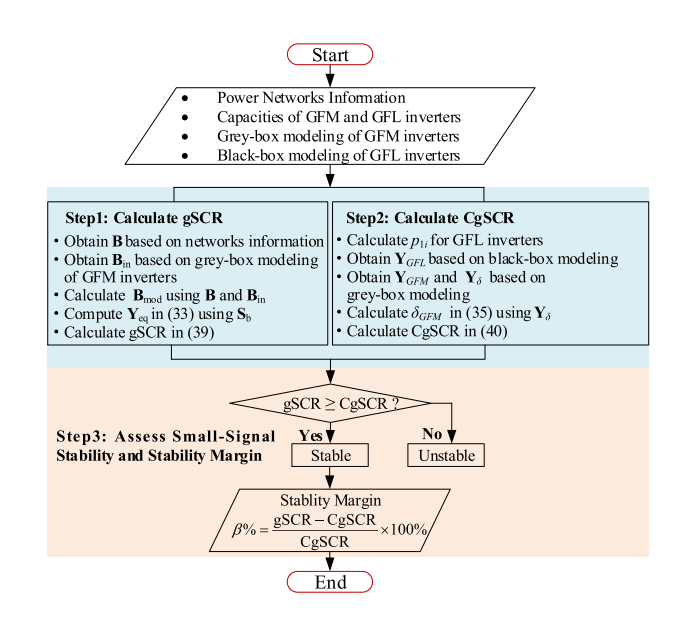


Fig. 6. Flowchart of the proposed method.

specific system (e.g., $\beta_0\%$ =20%). Especially, when $\beta_0\%$ is set as zero, gSCR=CgSCR and thus the system operates at the small-signal stability boundary.

The implementation of the proposed method is illustrated in Fig. 6, and its major steps are summarized below. Particularly, the proposed method is applicable to grey- and black-box inverter model due to the intellectual property concern.

Step 1: Calculate the gSCR based on $Y_{\rm eq}$ by (39). Matrix $Y_{\rm eq}$ in (33) can be obtained by combining matrix $\mathbf{B}_{\mathrm{mod}}$ with the capacity ratio matrix \mathbf{S}_{b} of all GFL inverters. Matrix $\mathbf{B}_{\mathrm{mod}}$ is the integration of matrix \mathbf{B} in (21) with matrix \mathbf{B}_{in} in (24). Matrix **B** can be obtained by the data of network topology; and matrix \mathbf{B}_{in} can be obtained from equivalent inductances L_{in} , which is related to the voltage source branch of GFM inverters, as shown in Fig. 5. L_{in} can be determined when only knowing parameters of the voltage and current control regulators of GFM inverters, as discussed in Section III-B, without disclosing all detailed state equations and control algorithms of these inverters. In the vendor's grey-box model of GFM inverters, these parameters can be provided to grid operators for system stability analysis [38]. Thus, the gSCR can be obtained by calculating the smallest eigenvalue of Y_{eq} . Step 2: Calculate the CgSCR based on (40). Firstly, the participation factor p_{1i} can be calculated based on (34) for all GFL inverters. Secondly, we obtain the frequency-domain functions $\mathbf{Y}_{GFL}(j\omega)$ and $\delta_{GFM}(j\omega)$ for GFL and GFM inverters. $\delta_{GFM}(j\omega)$ in (35) can be obtained based on $\mathbf{Y}_{\delta}(j\omega)$ and power networks information in Step 1. \mathbf{Y}_{δ} ($j\omega$) is the virtual apparatus branches of GFM inverters, as shown in Fig. 5, and can be obtained using $\mathbf{Y}_{GFM}(j\omega)$ and $B_{in} = 1/(\omega_0 L_{in})$. L_{in} can be obtained in Step 1. $\mathbf{Y}_{GFM}(j\omega)$ and $\mathbf{Y}_{GFL}(j\omega)$ are the admittance spectrum models of GFM and GFL inverters, respectively, which can be obtained by frequency-domain scanning [37] if they are modeled by black-box inverter modeling. Finally, with $\mathbf{Y}_{GFL}(j\omega)$ and $\delta_{GFM}(j\omega)$, we determine the CgSCR by

changing the capacity of any one inverter to adjust gSCR* in (40). When the $\mathbf{Y}_{GFL}(j\omega)$ and $\delta_{GFM}(j\omega)$ within the sideband of fundamental frequency [19] can satisfy the characteristic equation of the most critical system in (40), the $\mathbf{Y}_{GFL}(j\omega_c)$ and $\delta_{GFM}(j\omega_c)$ can be obtained. Thus, the gSCR* can be determined as CgSCR according to (40).

Step 3: Assess the system stability and the normalized system stability margin $\beta\%$ in (41) based on gSCR and CgSCR calculated in Steps 1 and 2.

The proposed method can be implemented quickly when the operation modes may change frequently in a practical system such as the disconnection of lines or the switching of apparatuses. The proposed gSCR can quickly be updated in Step 1, by modifying the network susceptance matrix **B** to tackle the changing network topology and interconnection relationship of inverters. Also, the proposed CgSCR can be conveniently updated in Step 2, which is determined based on the participation factor p_{1i} and grey- and black-box models of inverters. The participation factor p_{1i} can be updated with the network susceptance matrix **B** changing; the grey-and black-box models of inverters in the proposed method are provided by the manufacturers at one time and do not need to be updated. Then, the proposed stability margin $\beta\%$ can be obtained. Thus, the proposed method can be readily with the changing operation conditions. This method is quite helpful for grid planners and operators to fast understand under what grid operation conditions the small-signal stability issues may arise and decide if further detailed analysis tools are required.

VII. SIMULATION RESULTS

In this section, the proposed method will be validated by modal analysis and electromagnetic transient simulation on a modified IEEE 39-bus system.

We create the modified IEEE 39-bus test system as shown in Fig. 7 using the MATLAB/Simulink. In the system, there are ten directly driven wind turbine with permanent magnet synchronous generators (PMSG). The machine-side inverter (MSI) and the grid-side inverter (GSI) of each PMSG are presented by the average model based on voltage source inverter. Since we focus on the oscillation instability within the bandwidth frequency of PLL of GSI, which has timescale much smaller than the power control loops of MSI, the MSI of each PMSG is further modeled as the constant power source, and the GSI is considered to determine the small-signal dynamics of the PMSG in our adopted model. This modeling is commonly effective [39], [40].

Eight of these wind generators are interfaced with GFL inverters at buses 30–37 while the other two wind generators are interfaced with GFM inverters at buses 38–39. The capacity of each GFL inverter is 1.5 MW, and the capacities of the GFM inverters 1–2 are 3MW and 6MW, respectively. The control parameters of these two GFM inverters are presented in Table IV of Appendix A, while the control parameters of all GFL inverters are shown in Table V of Appendix A We set the PLL Proportional-Integrational (P-I) control parameters of GFL inverters 1~2 as "103.6,5368", GFL inverters 3~4 as "94.9,4510",

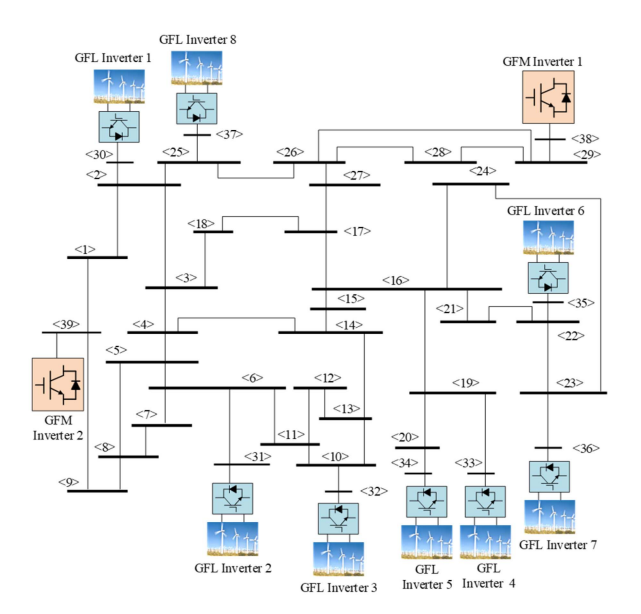


Fig. 7. One-line diagram of the modified IEEE 39-bus test system.

GFL inverters $5\sim6$ as "86.3,3727", and GFL inverters $7\sim8$ as "77.7,3019". The control parameters of voltage and current PI regulator of GFM inverters $1\sim2$ are set as those in Table I under cases 1 and 4, respectively. The parameters of the power network in the modified system are the same as those in the standard IEEE 39-bus system, and they can be found in [33]. It should be noted that though our method is derived based on the line reactance, its effectiveness will be demonstrated in the modified system, where both line resistance and reactance are considered in the power network.

A. Validation By Modal Analysis

1) Validation of Decoupling Scheme: First, we validate the proposed decoupling scheme that can preserve the main information of the entire 100% IBPS for the small-signal stability analysis. To this end, the modal analysis is applied to several cases in the modified IEEE 39-bus system. These numerical cases are created in the system by a scaling parameter k, which is used to equally increase (or reduce) all line impedances in the power network at the same time. When increasing the parameter k from 0.90 to 1.02, we compare the differences between the dominant eigenvalues in the entire 39-bus system and those in the formulated most critical subsystem based on the decoupling scheme (i.e., σ_1 and σ_2). The results are presented in Fig. 8 and Table II. The relative error ε between σ_1 and σ_2 is evaluated by $\varepsilon\% = (|\sigma_2 - \sigma_1|/|\sigma_1|) \times 100\%$.

The results of Fig. 8 and Table II validate that the small-signal stability of the entire system described by (25) can be approximately characterized by the most critical subsystem described by (35). It can be seen from Table II that the relative error between σ_1 and σ_2 is smaller than 5.8% in either stable or unstable system conditions. This validates the main information of the entire 100% IBPS, necessary for the small-signal stability assessment,

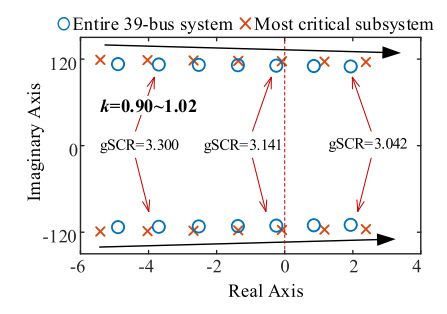


Fig. 8. Dominant eigenvalues of the modified 39-bus system and its most critical subsystem when increasing parameter k from 0.90 to 1.02.

TABLE II COMPARISON OF DOMINANT EIGENVALUES OF THE MODIFIED IEEE-39 BUS SYSTEM AND ITS MOST CRITICAL SUBSYSTEM

k	Entire system Results σ_1	Subsystem Results σ_2	Relative Error ε %
0.90	-4.9±j113.0	−5.4±j118.9	5.24%
0.92	−3.7± <i>j</i> 112.5	-4.0±j118.4	5.25%
0.94	-2.5±j112.0	-2.7±j117.9	5.27%
0.96	-1.4±j111.4	−1.4±j117.4	5.39%
0.98	−0.2±j110.9	±j116.9	5.41%
1.00	0.9±j110.4	1.2±j116.4	5.44%
1.02	2.0±j109.8	2.6±j115.9	5.74%

TABLE III RESULTS OF THE PROPOSED METHOD IN THE MODIFIED IEEE-39BUS SYSTEM

k	gSCR	CgSCR	Stability	Stability Margin β%
0.90	3.356	3.141	Stable	6.84%
0.92	3.300	3.141	Stable	5.06%
0.94	3.245	3.141	Stable	3.33%
0.96	3.192	3.141	Stable	1.62%
0.98	3.141	3.141	Stable	0%
1.00	3.092	3.141	Unstable	-
1.02	3.042	3.141	Unstable	-

can be captured by the formulated most critical subsystem based on the decoupling scheme very well.

2) Validation of Proposed Method: Then, we validate the proposed grid strength assessment method by the modal analysis in the modified IEEE 39-bus system. When increasing parameter k from 0.90 to 1.02, we calculate the values of gSCR by (39), and the values of CgSCR calculated by (40). The calculation results in each case are shown in Table III

The results of Fig. 8 and Table III verify the effectiveness of the proposed method for assessing grid strength in terms of the small-signal stability and stability margin of the system. As shown in Fig. 8 and Table III, when gSCR = CgSCR (i.e., $\beta\%=0$), the system dominant eigenvalues are exactly at the imaginary axis, which indicates the system is critically stable. When gSCR is larger than CgSCR (i.e., $\beta\%>0$), the system dominant eigenvalues in the left half of the complex plane, which suggests the system is stable and has a certain stability margin. When gSCR is smaller than CgSCR, the system dominant eigenvalues are in the right half of the complex plane, which means the system is unstable. Thus, the small-signal stability and stability margin of the system can be identified by comparing the gSCR with the CgSCR.

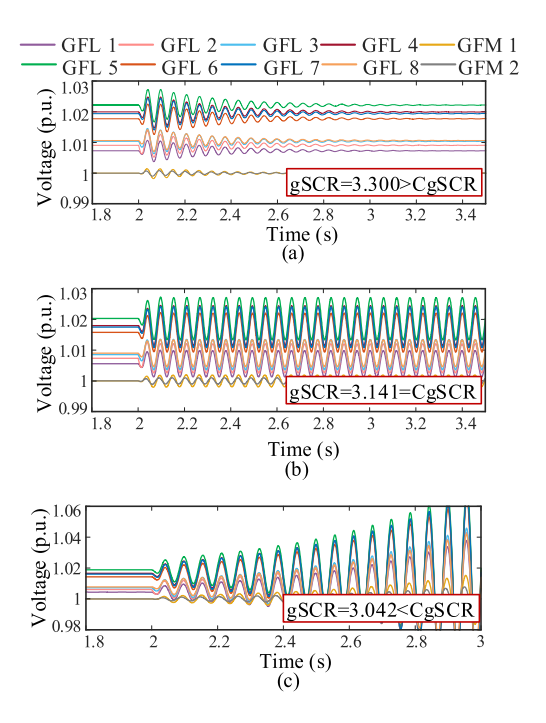


Fig. 9. Voltage trajectories of all inverter terminals in the modified 39-bus system when (a) gSCR = 3.300, (b) gSCR = 3.141, and (c) gSCR = 3.042.

B. Validation By Electromagnetic Transient Simulation

In the modified IEEE 39-bus system, the proposed method is further verified by electromagnetic time-domain simulation using MATLAB/Simulink with simulation time step 1e-5s. When coefficient k is set as 0.92, 0.98, and 1.02, the evaluation results of gSCR are 3.300, 3.141 and 3.042. Under these conditions, a sudden increase in load current is applied at 2.0 s to bus 31 and then is cleared at 2.02 s in the system. Fig. 9 shows the voltage trajectories of ten inverter terminals when gSCR = 3.300, 3.141and 3.042, respectively. It can be observed from Fig. 9 that when $gSCR = 3.300 \ge CgSCR = 3.141$, there are the convergence (or undamped) oscillations, which indicate the entire system is stable (or critically stable); when gSCR = 3.042 < CgSCR, the divergent oscillation can be seen, which means the entire system is unstable. The observations from Fig. 9 are consistent with those from Fig. 8 by modal analysis. This verifies the effectiveness of the proposed method.

VIII. CONCLUSION

This paper presented a method for evaluating grid strength in terms of the small-signal stability in the 100% IBPS dominated by GFL and GFM inverters. To reduce the analysis complexity, we first formulated a multi-inverter system modeling for the 100% IBPS and transformed it into a set of equivalent subsystems for the small-signal stability analysis. Then, based on the analysis results, an index and its threshold were proposed to assess grid strength in terms of small-signal stability and stability margin. The proposed index was defined based on an equivalent network impedance that included the voltage support characteristics of GFM inverters. The threshold of the proposed index was defined by including the small-signal dynamics of

TABLE IV
PARAMETERS OF THE GFM INVERTER IN THE TEST SYSTEM

Apparatus Base Values for Per-unit Calculation		
f_{base} =50Hz U_{b} =0.69kV S_{base} = 1.5 MW		
Parameters of the Inverter Filter (per-unit values)		
$L_{\rm f} = 0.05$ $C_{\rm f} = 0.05$ $L_{\rm g} = 0.06$		
Parameters of the GFM-Based Control (per-unit values)		
PI parameters of the current control Loop: $K_{pi}=0.3$, $K_{ii}=10$		
PI parameters of the voltage control Loop: $K_{pv}=2$, $K_{iv}=30$		
Parameters of the swing equation: $J = 2$, $D = 20$		
Parameters of first-order filters: $T_{\text{vf}} = 0.002$, $K_i = 1$, $T_P = 0.2$, $k_P = 1.0$		

 $\label{thm:constraint} TABLE\ V$ Parameters of the GFL Inverter in the Test System

	Apparatus Base Values for Per-unit Calculation
	f_{base} =50Hz U_{b} =0.69kV S_{base} = 1.5 MW
	Parameters of the GFL Control (per-unit values)
	PI parameters of the current control Loop: 0.3, 10
Ti	me coefficient of voltage feedforward first-order filter: 0.01
	PI parameters of the dc voltage control Loop: 0.5, 40
	PI parameters of the PLL: 103.8, 5391

both GFL and GFM inverters. An analytical expression was derived to determine the threshold instead of empirical reasoning or electromagnetic transient simulations based on trial and error. The expression cannot only characterize the small-signal stability boundary of the 100% IBPS, but it can also analyze the impact of GFL and GFM inverter dynamics on the stability boundary. With the proposed index and its threshold, our method was proposed and then validated on a modified IEEE 39-bus system. This proposed method will be helpful for guiding grid planning and operation to address the small-signal stability issues in a 100% IBPS with GFL and GFM inverters. Our future works will evaluate the grid strength of the 100% IBPS in terms of large-signal stability, where behaviors of GFL and GFM inverters significantly alter due to controller limits.

APPENDIX

A. System Parameters

B. Derivation of
$$\mathbf{Y}_{GFM}(s)$$
 in (19) and $\mathbf{Y}_{\delta}(s)$ in (20)

This appendix explains how to derive the admittance of the GFM inverter in the global *xy*-frame.

Submitting (16) into (11), dynamics of the GFM inverter in the global *xy*-frame can be expressed:

$$-\Delta \mathbf{V}_{xy} = \mathbf{Z}_{dq}(s)\Delta \mathbf{I}_{xy} + (\mathbf{Z}_{dq}(s)\mathbf{I}_0 + \mathbf{V}_0)\Delta\theta \tag{42}$$

where $\mathbf{Z}_{dq}(s) = \mathbf{Y}^{-1}{}_{dq}(s)$ represents the dq-frame impedance of the GFM inverter which can be derived by (15).

For simplicity, we consider that $P_E = V_d I_d + V_q I_q$, and note that the voltage source property of the GFM inverter, that is, V_d is nearly constant and $V_q = 0$ within the voltage-loop bandwidth [7]. Thus, the angle dynamics in (18) can be rewritten:

$$\Delta\theta \approx -\frac{F_P(s)}{Js^2 + Ds} \Delta I_d \tag{43}$$

Substituting (43) and (16) into (42) yields

$$\Delta \mathbf{V}_{xy} = -(\mathbf{Z}_{dq}(s) + \mathbf{Z}_{\theta}(s))\Delta \mathbf{I}_{xy} \tag{44}$$

$$\mathbf{Z}_{\theta}(s) = -\frac{F_{P}(s)(\mathbf{Z}_{dq}(s)\mathbf{I}_{0} + \mathbf{V}_{0})}{Js^{2} + Ds + F_{P}(s)I_{q0}}[1\ 0]$$
(45)

Then, the *xy*-frame admittance of the GFM inverter in (19) can be obtained

$$\mathbf{Y}_{GFM}(s) = -(\mathbf{Z}_{dq}(s) + \mathbf{Z}_{\theta}(s))^{-1} \tag{46}$$

Also, a detailed expression of the second part in (20) becomes $\mathbf{Y}_{\delta}(s) = (\mathbf{Z}_{dq}(s) + \mathbf{Z}_{\theta}(s))^{-1} - \mathbf{Z}^{-1}_{dq}(s)$.

C. Deformation of Characteristic Equation in (28)

The Schur complement of (27) can be deduced

$$0 = -diag\{S_{bi}\mathbf{F}^{-1}\mathbf{Y}_{GFL,i}(s)\} + \mathbf{B}_{1} \otimes \mathbf{I}_{2} - [\mathbf{B}_{2} \otimes \mathbf{I}_{2}][diag\{S_{bm,j}\mathbf{F}^{-1}\mathbf{Y}_{\delta,j}(s)\} + \tilde{\mathbf{B}}_{4} \otimes \mathbf{I}_{2}]^{-1}[\mathbf{B}_{2}^{\top} \otimes \mathbf{I}_{2}]$$

$$(47)$$

Then, the part $[diag\{S_{bm,j}\mathbf{F}^{-1}\mathbf{Y}_{\delta,j}(s)\} + \tilde{\mathbf{B}}_4 \otimes \mathbf{I}_2]^{-1}$ also can be deformed based on Woodbury matrix identity [34]:

$$\left[\tilde{\mathbf{B}}_{4} \otimes \mathbf{I}_{2} + diag\{S_{bm,j}\mathbf{F}^{-1}\mathbf{Y}_{\delta,j}(s)\}\right]^{-1} = \tilde{\mathbf{B}}_{4}^{-1} \otimes \mathbf{I}_{2} + \Delta(s)$$
(48)

in which the remainder $\Delta(s)$ has been formulated as (31). By substituting (48) into (47), (28) will be obtained.

REFERENCES

- X. Zhao et al., "Challenges toward carbon neutrality in China: Strategies and countermeasures," Resour., Conservation Recycling, vol. 176, Jan. 2022, Art. no. 105959.
- [2] L. Bird, M. Milligan, and D. Lew, "Integrating variable renewable energy: Challenges and solutions," Tech. Rep. NREL/TP-6A20-60451, 1097911, Sep. 2013.
- [3] A. S. Brouwer et al., "Impacts of large-scale intermittent renewable Energy sources on electricity systems, and how these can be modeled," *Renewable Sustain. Energy Rev.*, vol. 33, pp. 443–466, May 2014.
- [4] M. Amin, A. Rygg, and M. Molinas, "Self-synchronization of wind farm in an MMC-based HVDC system: A stability investigation," *IEEE Trans. Energy Convers.*, vol. 32, no. 2, pp. 458–470, Jun. 2017.
- [5] M. Zhao, X. Yuan, J. Hu, and Y. Yan, "Voltage dynamics of current control time-scale in a VSC-connected weak grid," *IEEE Trans. Power* Syst., vol. 31, no. 4, pp. 2925–2937, Jul. 2016.
- [6] L. Huang et al., "Grid-synchronization stability analysis and loop shaping for PLL-based power converters with different reactive power control," *IEEE Trans. Smart Grid*, vol. 11, no. 1, pp. 501–516, Jan. 2020.
- [7] Y. Gu and T. C. Green, "Power system stability with a high penetration of inverter-based resources," *Proc. IEEE*, vol. 111, no. 7, pp. 832–853, Jul. 2023.
- [8] H. Liu et al., "Subsynchronous interaction between direct-drive PMSG based wind farms and weak AC networks," *IEEE Trans. Power Syst.*, vol. 32, no. 6, pp. 4708–4720, Nov. 2017.
- [9] J. Z. Zhou, H. Ding, S. Fan, Y. Zhang, and A. M. Gole, "Impact of short-circuit ratio and phase-locked-loop parameters on the small-signal behavior of a VSC-HVDC converter," *IEEE Trans. Power Del.*, vol. 29, no. 5, pp. 2287–2296, Oct. 2014.
- [10] C. Yang, L. Huang, H. Xin, and P. Ju, "Placing grid-forming converters to enhance small signal stability of PLL-integrated power systems," *IEEE Trans. Power Syst.*, vol. 36, no. 4, pp. 3563–3573, Jul. 2021.
- Trans. Power Syst., vol. 36, no. 4, pp. 3563–3573, Jul. 2021.
 [11] D. B. Rathnayake et al., "Grid forming inverter modeling, control, and applications," *IEEE Access*, vol. 9, pp. 114781–114807, 2021.
- [12] J. Rocabert, A. Luna, F. Blaabjerg, and P. Rodríguez, "Control of power converters in AC microgrids," *IEEE Trans. Power Electron.*, vol. 27, no. 11, pp. 4734–4749, Nov. 2012.
- [13] J. Lyu et al., "Sub-synchronous oscillation mechanism and its suppression in MMC-based HVDC connected wind farms," *IET Gen., Transmiss. & Distrib.*, vol. 12, no. 4, pp. 1021–1029, Feb. 2018.

- [14] U. Markovic et al., "Partial grid forming concept for 100% inverter-based transmission systems," in *Proc. IEEE Power Energy Soc. Gen. Meeting*, 2018, pp. 1–5.
- [15] R. Rosso, S. Engelken, and M. Liserre, "Robust stability investigation of the interactions among grid-forming and grid-following converters," *IEEE J. Emerg. Sel. Topics Power Electron.*, vol. 8, no. 2, pp. 991–1003, Jun. 2020.
- [16] S. Gomes, N. Martins, and C. Portela, "Computing small-signal stability boundaries for large-scale power systems," *IEEE Trans. Power Syst.*, vol. 18, no. 2, pp. 747–752, May 2003.
- [17] C. E. Ugalde-Loo, J. B. Ekanayake, and N. Jenkins, "State-space modeling of wind turbine generators for power system studies," *IEEE Trans. Ind. Appl.*, vol. 49, no. 1, pp. 223–232, Jan./Feb. 2013.
- [18] Y. Gu and T. C. Green, "Reduced-order models for representing converters in power system studies," *IEEE Trans. Power Electron.*, vol. 33, no. 4, pp. 3644–3654, Apr. 2018.
- [19] X. Wang and F. Blaabjerg, "Harmonic stability in power electronic-based power systems: Concept, modeling, and analysis," *IEEE Trans. Smart Grid.*, vol. 10, no. 3, pp. 2858–2870, May 2019.
- [20] Y. Liao, H. Wu, X. Wang, M. Ndreko, R. Dimitrovski, and W. Winter, "Stability and sensitivity analysis of multi-vendor, multi-terminal HVDC systems," *IEEE Open J. Power Electron.*, vol. 4, pp. 52–66, Jan. 2023.
- [21] H. Liu, X. Xie, and W. Liu, "An oscillatory stability criterion based on the unified dq -frame impedance network model for power systems with high-penetration renewables," *IEEE Trans. Power Syst.*, vol. 33, no. 3, pp. 3472–3485, May 2018.
- [22] P. Kundur, Power System Stability and Control. New York, NY, USA: McGraw-Hill, 1994.
- [23] NERC, "Reliability guideline: Integrating inverter-based resources into low short circuit strength systems," North Amer. Elect. Rel. Corporation, Jun. 2017. [Online]. Available: http://www.nerc.com/pa/RAPA/rg/ ReliabilityGuidelines
- [24] Y. Zhang, S.-H. Huang, J. Schmall, J. Conto, J. Billo, and E. Rehman, "Evaluating system strength for large-scale wind plant integration," in *Proc. IEEE PES Gen. Meeting* | *Conf. Expo.*, Jul. 2014, pp. 1–5.
- [25] R. Fernandes, S. Achilles, and J. MacDowell, "Minnesota renewable energy integration and transmission study final report," in *Proc. GE Energy Consulting*, Schenectady, NY, USA, Oct. 2014.
- [26] CIGRE, "Connection of wind farms to weak AC networks," TGS, CIGRE WG B4-62, 2017.
- [27] IEEE Standard for Interconnection and Interoperability of Inverter-Based Resources (IBRs) Interconnecting with Associated Transmission Electric Power Systems, IEEE Standard 2800–2022, 2022.
- [28] W. Dong, H. Xin, D. Wu, and L. Huang, "Small signal stability analysis of Multi-infeed power electronic systems based on grid strength assessment," *IEEE Trans. Power Syst.*, vol. 34, no. 2, pp. 1393–1403, Mar. 2019.
- [29] S. D'Arco and J. A. Suul, "Equivalence of virtual synchronous machines and frequency-droops for converter-based MicroGrids," *IEEE Trans. Smart Grid.*, vol. 5, no. 1, pp. 394–395, Jan. 2014.
- [30] Y. Gu, Y. Li, Y. Zhu, and T. C. Green, "Impedance-based whole-system modeling for a composite grid via embedding of frame dynamics," *IEEE Trans. Power Syst.*, vol. 36, no. 1, pp. 336–345, Jan. 2021.
- [31] L. Huang et al., "Impacts of grid structure on PLL-synchronization stability of converter-integrated power systems," *IFAC-PapersOnLine*, vol. 55, no. 13, pp. 264–269, 2022.
- [32] G.W. Stewart, "Matrix perturbation theory," 1990.
- [33] "IEEE PES task force on Benchmark systems for stability controls," Nov. 2013. Available: [Online]. Available: http://www.sel.eesc.usp.br/ ieee/
- [34] N. J. Higham, Accuracy and Stability of Numerical Algorithms, 2nd ed. Philadelphia, PA, USA: S I AM, 2002.
- [35] Y. Zhou et al., "Small-signal stability assessment of heterogeneous gridfollowing converter power systems based on grid strength analysis," *IEEE Trans. Power Syst.*, vol. 38, no. 3, pp. 2566–2579, May 2023.
- [36] IEEE Guide for Planning DC Links Terminating at AC Locations Having Low Short-Circuit Capacities, IEEE Standard 1204–1997, 1997.
- [37] A. Rygg, M. Molinas, C. Zhang, and X. Cai, "A modified sequence-domain impedance definition and its equivalence to the dq-domain impedance definition for the stability analysis of AC Power Electronic Systems," *IEEE J. Emerg. Sel. Topics Power Electron.*, vol. 4, no. 4, pp. 1383–1396, Dec. 2016.
- [38] Y. Zhu, Y. Gu, Y. Li, and T. Green, "Participation analysis in impedance models: The grey-box approach for power system stability," *IEEE Trans. Power Syst.*, vol. 37, no. 1, pp. 343–353, Jan. 2022.

- [39] B. Liu, Z. Li, X. Zhang, X. Dong, and X. Liu, "Impedance-based analysis of control interactions in weak-grid-tied PMSG wind turbines," *IEEE J. Emerg. Sel. Topics Circuits Syst.*, vol. 11, no. 1, pp. 90–98, Mar. 2021.
- [40] J. Hu, Q. Hu, B. Wang, H. Tang, and Y. Chi, "Small signal instability of PLL-synchronized type-4 wind turbines connected to high-impedance AC grid during LVRT," *IEEE Trans. Energy Convers.*, vol. 31, no. 4, pp. 1676–1687, Dec. 2016.



Fuyilong Ma received the B.Eng. degree in electrical engineering from the College of Electrical Engineering, Zhejiang University, Hangzhou, China, in 2019. He is currently working toward the Ph.D. degree with the College of Electrical Engineering, Zhejiang University, Hangzhou. His research interests include renewable energy integration, fundamental theories for dynamic analysis, and control of power-electronic-based renewable power systems.



Huanhai Xin (Senior Member, IEEE) received the Ph.D. degree from the College of Electrical Engineering, Zhejiang University, Hangzhou, China, in 2007. From June 2009 to July 2010, he was a Postdoctor with the Electrical Engineering and Computer Science Department, University of Central Florida, Orlando, FL, USA. He is currently a Professor with the Department of Electrical Engineering, Zhejiang University. His research focuses on renewable power system stability analysis and control.



Di Wu (Member, IEEE) received the B.S. and M.S. degrees in electrical engineering from the Kunming University of Science and Technology, Kunming, China, and Zhejiang University, Hangzhou, China, in 2002 and 2005, respectively, the Ph.D. degree in the area of applied complex networks from the Polytechnic University of Turin, Turin, Italy, in 2011, and the Ph.D. degree in power system engineering from Zhejiang University. He is currently an Associate Professor with the Department of Electrical and Computer Engineering, North Dakota State University,

Fargo, ND, USA. His research interests include renewable energy integration, power system dynamics and stability, cascading failures, and application of complex network theory in power grids.



Yun Liu (Senior Member, IEEE) received the B.Eng. (with First Class Hons.) and Ph.D. degrees from the College of Electrical Engineering, Zhejiang University, Hangzhou, China, in 2011 and 2016, respectively. His work experience includes the University of Central Florida, Orlando, FL, USA, Nanyang Technological University, Singapore, and Shenzhen University. He is currently an Associate Professor with the School of Electric Power Engineering, South China University of Technology, Guangzhou, China. His research interests include stability analysis of

renewable power system, cyber-physical smart grid, and distributed control/optimization. He is also an Associate Editor for *IET Smart Grid*.



Xia Chen received the B.S. degree in power system and its automaton from the Wuhan University of Technology, Wuhan, China, in 2006, and the M.S. and Ph.D. degrees in electrical engineering from the Huazhong University of Science and Technology (HUST), Wuhan, China, in 2008 and 2012, respectively. From 2012 to 2015, she was a Postdoctoral Research Fellow with the University of Hong Kong, Hong Kong. In 2015, she joined the HUST, where she is currently an Associate Professor with the School of Electrical and Electronic Engineering. Her research

interests include distributed control technology, renewable energy integration technologies, and new smart grid device.